

LOBSTER EYES AS X-RAY TELESCOPES

J. R. P. ANGEL

Steward Observatory, University of Arizona
 Received 1979 February 7; accepted 1979 April 12

ABSTRACT

A new optical configuration for grazing-incidence, imaging X-ray telescopes is described, one that is similar to the reflective eyes of macruran crustaceans such as lobsters. The field of view can be made as large as desired, and it is practical to achieve good efficiency for photon energies up to 10 keV. Spatial resolution of a few seconds of arc over the full field is possible, in principle, if very small reflecting cells can be fabricated.

Two model telescopes are described. The first has a field similar to that of optical Schmidt telescopes (8°), an aperture of 2.5 m, and a spatial resolution of $30''$. In a 2 year mission it would survey the entire sky to the limiting sensitivity of the *Einstein* telescope, and it has the advantage of good response at the 7 keV iron emission lines. The second telescope, an all-sky monitor with a 2π sr field of view, is a hemisphere 3 m in diameter. It reaches the limiting sensitivity of *Uhuru* in ~ 1 hour with positions accurate to $\sim 2'$, and can detect and locate quite faint burst sources.

Subject headings: instruments — X-rays: general

I. INTRODUCTION

Two types of imaging, grazing-incidence telescopes are currently used in X-ray astronomy. High-resolution reflectors have been built following the designs of Wolter (1952), in which the X-rays are first incident on a parabola of revolution and then reflected a second time by a hyperboloid of revolution to come to a focus. Adequate collection area is obtained by nesting the surfaces one within another (Giacconi and Rossi 1960), and images with a resolution of a few seconds of arc have been obtained by solar telescopes (Vaiana *et al.* 1974) and with the *HEAO 2* (*Einstein*) satellite (Van Speybroek 1977). Another type of optics using two plates curved in only one dimension was suggested by Kirkpatrick and Baez (1948). This design again relies on two reflections. In imaging telescopes, an upper assembly of many curved plates is arranged to direct the X-rays toward a linear focus, whereupon a second array oriented perpendicularly redirects the rays toward a true imaging focus. Telescopes of this type have been used in sounding rocket observations by Gorenstein *et al.* (1975) and others. Designs of both types of reflectors have been extensively reviewed in the literature (e.g., Gursky and Schwartz 1974; Underwood 1975).

Grazing angles of about 1° have been used in the highest energy telescopes, giving response up to a photon energy of ~ 4 keV. The field of view in both designs is approximately equal to the grazing angle, and their spatial resolution drops to about $1'$ for sources $\sim 30'$ off axis. A deficiency in these telescopes is their complete lack of sensitivity in the region 6–7 keV, where the strong iron K line emission is present in many sources. This line is the only spectral feature in the X-ray region that can be detected unambiguously with sensitive proportional counter detectors.

Wolter or Kirkpatrick-Baez telescopes of grazing angles small enough to detect iron lines could be constructed, but would have very small effective area and field of view.

A focusing device which overcomes the restricted angular field of the above designs has been proposed by Schmidt (1975). He points out that a "venetian blind" of flat reflecting plates tilted radially toward a common line makes a one-dimensional image over the surface of a cylinder concentric with the line, with unrestricted field of view. Schmidt also considered a configuration in which two venetian blind sets of plates were arranged at right angles to give a two-dimensional focus. In this configuration, though, there is a preferred axis, and the field of view, though larger than that of a cross-plate telescope, is still restricted by off-axis aberrations.

In this paper we describe a new type of grazing-incidence telescope, which combines high-energy response and wide field of view. The optics are based on the reflective eyes of macruran crustaceans (lobsters, shrimps, and crayfishes). The principle of imaging of these eyes has only recently been understood, and was discovered by Vogt (1975) and Land (1978). The eyes consist in essence of many small tubes, of square cross section and with reflective internal surfaces, arranged over a spherical surface with their axes radial, as in Figure 1. Light from many tubes is reflected to form a single image on a spherically curved retina with half the radius of the cell surface. A true image is formed by rays which reflect twice off adjacent walls on passing through a square cell, as shown in Figure 2. Such rays have the property that the reflected ray is in the plane of the incident ray and the cell axis, and that the incoming and emerging rays are at the same angle to the cell axis. Since all cell axes are radial from a common point, these two

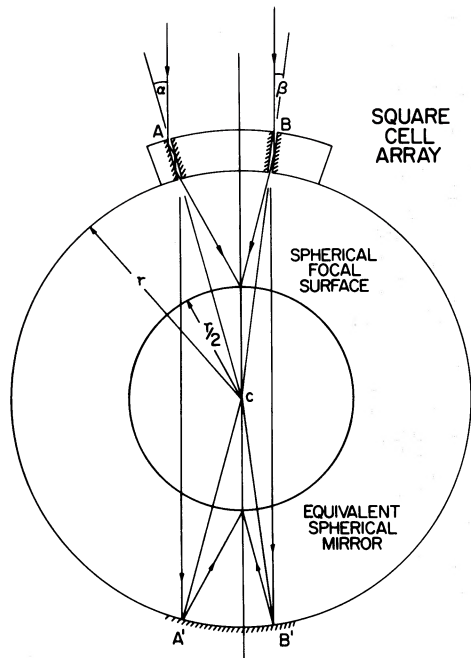


FIG. 1.—Representation of how reflected light is brought to a focus. True focusing requires an odd number of reflections in both x - and y -directions. The lower part of the diagram shows how reflection at a normal spherical mirror has the identical geometry.

conditions result in a focus exactly analogous to that of a spherical mirror, where reflection is in the plane of the incident ray and the mirror normal. Singly reflected rays are focused on one dimension only, and form two linear images parallel to the cell sides, and passing through the point focus.

In the crustacean eyes the square cells are short, with length equal to about twice their width, and reflection takes place over a large range of angles of incidence to form a rather fast focus. For X-ray applications the cells must be made very long, with length about 100 times the width, but the optical principle remains the same. It is closely related to that of Schmidt's two-dimensional device, except that by merging the two orthogonal sets of plates and adopting spherical rather than cylindrical symmetry, the preferred axis is removed and the field of view can be as large as desired. The eye of a lobster, for example, has a field of view of slightly more than 180° .

At first sight it would appear that the superposition of a true-focused and a linear-focused image would be a substantial drawback. However, we argue that the limiting sensitivity is only slightly reduced by the additional background of the line images, while the response to high-energy X-rays is considerably enhanced, as is the effective area for spectroscopy of sources of moderate brightness. The optics are described in detail in § II, with a discussion of effective collecting area at different X-ray wavelengths. A laboratory model is described in § III, and in § IV applications to X-ray astronomy are discussed,

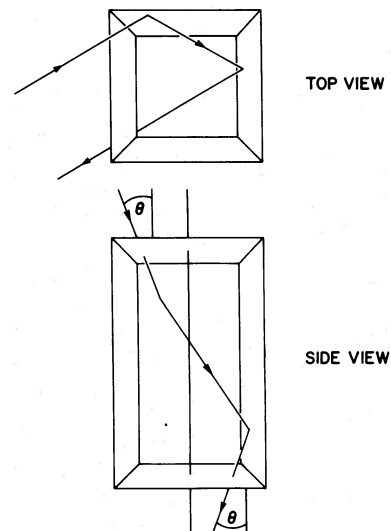


FIG. 2.—A ray passing through a cell with two reflections off adjacent walls. Such a ray is brought to the true focus.

together with the performance of two telescopes suitable for shuttle launch.

II. THE OPTICS

The basic optical element we considered is a tube of square cross section and plane-parallel mirror sides. For our application with very long cells, the mirror walls of the cell must be exactly parallel to form good images at long wavelengths when multiple reflections are important. Looking into such a cell we see a checker pattern of reflections in the plane of the far end, as shown in Figure 3. Each square image is

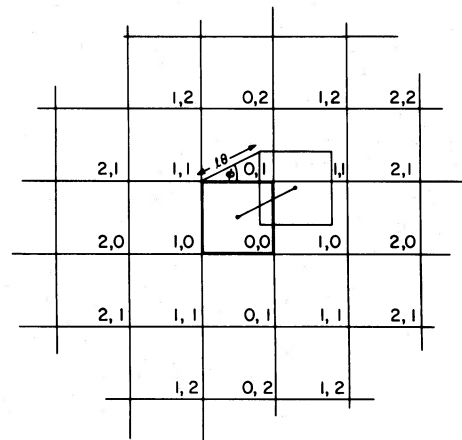


FIG. 3.—Pattern of multiple reflections seen from the walls of the basic square cell. The displaced square at (θ, ϕ) represents the top of the cell as seen by a distant observer. The area of each of the four labeled squares covered by the top square shows how the incoming light is distributed among four possible emergent directions. The numbers in each square give the number of reflections from the vertical and horizontal walls, respectively. The emergent direction is related to the number of reflections as discussed in the text.

labeled with an integer (x, y) -coordinate, which indicates the number of reflections off the vertical and horizontal walls which yield that image. Consider the box axis oriented at an arbitrary direction (θ, ϕ) to incoming parallel light. There will in general be partial reflections in each of four different directions. Figure 3 shows the square front of the box displaced at $(l\theta, l\phi)$ to the back plane pattern, as it would appear when viewed from the incoming light direction for small θ . The four regions within this square show how the light incident on the front aperture is shared among four reflection paths for the emerging beam directions. The two grazing angles of incidence are $\theta \cos \phi$ on the vertical walls and $\theta \sin \phi$ on the horizontal walls. The emergent directions are $\theta \cos \phi$ (-1) ^{n_x} horizontally from the box axis and $\theta \sin \phi$ (-1) ^{n_y} vertically, where n_x is the number of reflections off vertical walls and n_y the number off horizontal walls. The net reflectivity for any given path is given by $R^{|n_x|}(\theta \cos \phi) \times R^{|n_y|}(\theta \sin \phi)$, where $R(\psi)$ is the reflection coefficient for light incident at grazing angle ψ . R is quite high up to some critical grazing angle θ_c , and falls rapidly for angles larger than this. For any given material, θ_c is proportional to X-ray wavelength. It follows that the net reflectivity for a path is small unless both $\theta \lesssim \theta_c$ and $|n_x| + |n_y|$ are not large.

We are now in a position to calculate the imaging properties of a telescope made from many boxes distributed over an inner spherical surface of radius r . The reflection geometry is illustrated in Figure 1. Two representative rays of parallel light from a distant source enter reflecting cells at A and B at angles α and β to the cell axes. The rays that undergo reflection from adjacent walls (in general, with both n_x and n_y odd) are both reflected in the plane of incidence, and, for small angles of incidence (paraxial condition), are brought to a focus on the sphere of radius $\frac{1}{2}r$. The geometry of reflection, and hence the aberrations, are exactly the same as for a concave spherical mirror of radius r . This can be seen from Figure 1, where we have continued the incoming rays to strike a concave mirror at A' and B'. In the application for X-ray astronomy, the grazing angles are necessarily small, and the spherical aberration will be very small (see below). The full image diameter for a stellar source will be equal to the cell diagonal. This is because the component contributing to the focus emerges as a parallel beam from the bottom of the cell, and will not spread out any more than the cell size. Because grazing angles must be small, the entrance pupil to the system is located at the center of curvature. There is no preferred axis, and the field of view can be made as large as desired simply by covering more of the sphere with square cells. There is no limit to the field of view as in a concave spherical mirror, because the focal plane does not obstruct incoming rays.

Those rays which undergo only one reflection (in general, an even number of reflections in one direction and an odd number in the other), on passing through the cell, will, if the cell squares are all similarly oriented, be brought to two perpendicular linear foci. Figure 1 shows correctly the geometry of singly and

triply reflected rays for a cross section perpendicular to the reflecting surfaces. The linear focus is perpendicular to the plane of the paper and passes through the true image. Rays passing directly through the cells without reflection (in general with n_x and n_y both even), of course, will not be focused at all, and will form a checkered patch centered on the true image.

a) Effective Area

The value of such a composite image for astronomy depends on the overall efficiency of imaging, and the relative energy and brightness of the spot, linear, and diffuse components. These characteristics are determined by the length-to-width ratio, l/w , of the boxes, and the reflectivity as a function of grazing angle of the reflective surfaces. An exact knowledge of the image for incoming parallel light would require numerical integration of the four rays from the back of every cell. A good analytical approximation for the component intensities, though, can be obtained by considering only a few cells distributed in a coarse grid. Consider first a square grid with angular separation between adjacent points of $\alpha = w/l$, subtended at the center of curvature. Take the center cell of the grid to lie on the incoming ray that passes through the center of curvature. With this choice of cells, all the light entering each paraxial cell is reflected in only one direction, and the sum for each image component is greatly simplified. We obtain the following effective areas in each component. For both n_x and n_y even (unfocused),

$$a_{ee}/a_o = (1 + 2R^2(2\alpha) + 2R^4(4\alpha) + 2R^6(6\alpha) + \dots)^2; \quad (1a)$$

for n_x even and n_y odd and vice-versa (horizontal and vertical images),

$$a_{eo}/a_o = a_{oe}/a_o = [1 + 2R^2(2\alpha) + 2R^4(4\alpha) + \dots] \times 2[R(\alpha) + R^3(3\alpha) + R^5(5\alpha) + \dots]; \quad (1b)$$

and for n_x and n_y both odd (true image),

$$a_{oo}/a_o = 4[R(\alpha) + R^3(3\alpha) + R^5(5\alpha) + \dots]^2, \quad (1c)$$

where a_o is the area of a cell. These series will give a good approximation if the critical angle $\theta_c \gg \alpha$. The effective area A of a telescope with filled frontal area for the different components is then given by

$$A_{ee} = (a_{ee}/a_o)r^2\alpha^2\eta, \quad (2)$$

and similarly for A_{eo} , A_{oe} , and A_{oo} , where r is the radius of curvature and η the open fraction of the frontal area.

At higher X-ray energies, where the reflectivity drops quickly, more cells are needed in the sum to give an accurate efficiency estimate. We have calculated the effective area for a finer square grid, of angular spacing equal to $\frac{1}{2}\alpha$, which is valid for wavelengths

with critical angle $\gtrsim \alpha$. The incoming light in each of these cells is shared between one, two, or four equal areas which are found by using diagrams like Figure 1. Summing the contributions from all reflections we obtain for the effective areas

$$a_{ee}'/a_o = [2 + R^2(3\alpha/2) + 2R^2(2\alpha) + R^2(5\alpha/2) + R^4(7\alpha/2) + 2R^4(4\alpha) + R^4(9\alpha/2) + \dots]^2; \quad (3a)$$

$$a_{oo}'/a_o = [R(\alpha/2) + 2R(\alpha) + R(3\alpha/2) + R^3(5\alpha/2) + 2R^3(3\alpha) + R^3(7\alpha/2) + \dots]^2; \quad (3b)$$

$$a_{eo}' = a_{oe}' = (a_{ee}'a_{oo}')^{1/2}. \quad (3c)$$

Since this grid has 4 times as many cells as previously used, the effective area for a filled mirror is now given by

$$A_{ee} = (a_{ee}'/a_o)r^2\alpha^2\eta/4 \text{ etc.} \quad (4)$$

At higher photon energies where $\theta_c < \alpha$, only those cells very close to the center cell contribute to the true focus, and both approximations given above break down. The reflectivity of good reflectors at high energies is near unity up to the critical angle θ_c , where it drops sharply. Making the approximation $R = 1$ for $\theta < \theta_c$ and 0 for $\theta > \theta_c$ and integrating over a full array of cells out to $\theta_x = \theta_y = \pm \theta_c$ we obtain for the effective area

$$A_{oo} \approx r^2\alpha^2\eta(\theta_c/\alpha)^4 \quad (\theta_c/\alpha \leq 1). \quad (5)$$

The choice of α thus determines the highest energy at the spot focus of the telescope, and the effective area falls steeply as λ^4 for wavelengths shorter than a critical wavelength λ_c , given by $\theta_c = \alpha$. In this domain the linear images contain more energy than the true focus. One can show that

$$A_{eo} + A_{oe} = 2r^2\alpha^2\eta(\theta_c/\alpha)^2 \quad (\theta_c/\alpha \leq 1). \quad (6)$$

The effective area for the whole cross image is thus $\frac{1}{2}r^2\alpha^2\eta$ at a wavelength $\lambda_c/2$, and $(2/9)r^2\alpha^2\eta$ at $\lambda_c/3$. We note that the area is independent of the cell geometry α , depending only on radius and frontal efficiency. The size of the cross does however depend on α , the full width at half-maximum (FWHM) of the cross arms being equal to $r\alpha$ at the detector. The average brightness of radiation in the cross is enhanced by a factor $\theta_c^2/\alpha\Delta\theta$, where $\Delta\theta$ is the angular resolution of the telescope. (Note that at low energies where multiple even reflections are important the cross is larger).

At wavelengths $\lesssim \frac{1}{2}\lambda_c$ the effective area for directly transmitted light, equal to $r^2\alpha^2\eta$, becomes larger than the total for the cross and spot components combined. The FWHM of the patch of directly transmitted light is again $r\alpha$ at the detector, projecting to 2α on the sky. We note that relation 3c is still valid for wavelengths less than critical, i.e., the effective area for each linear focus is equal to the geometric mean of the areas for the spot and diffuse components.

To proceed further, effective areas for a mirror made of a specific material are needed, and we show here results calculated for nickel. This is commonly used for telescopes operating at wavelengths of a few angstroms, because it is a stable material with a relatively large θ_c , high reflectivity, and freedom of absorption bands. We have calculated the reflectivity for wavelengths in the range 1.5–10 Å and grazing angles 12.5–200' according to the theory conveniently summarized by Underwood (1975), and values are given in Table 1. With these values of reflectivity we have computed and plotted in Figure 4 the values of A_{ee} and A_{oo} for $l/w = 68.8$ ($\alpha = 50'$) and $l/w = 137.5$ ($\alpha = 25'$). The geometric mean of A_{ee} and A_{oo} , A_{eo} , is not plotted. Above the critical energy the effective area is computed from equation (5), using the value $\theta_c = \lambda/16.5$ (Å) for nickel.

The effective areas for all four image components are approximately equal at low energy, and again at the energy corresponding to $\theta_c = \alpha$. At this critical energy E_c , equal to 8.2 keV for $\alpha = 25'$ and 4.1 keV

TABLE 1
THEORETICAL REFLECTIVITY OF NICKEL

GRAZING ANGLE OF INCIDENCE (arcmin)	WAVELENGTHS (Å)							
	1.5	2	2.5	3	4	5	7	10
12.5	0.978	0.976	0.972	0.969	0.963	0.958	0.950	0.942
25	0.516	0.934	0.935	0.933	0.924	0.916	0.901	0.886
37.5	0.020	0.123	0.826	0.871	0.875	0.869	0.851	0.832
50	0.005	0.020	0.077	0.437	0.800	0.811	0.798	0.779
62.5	...	0.008	0.024	0.072	0.590	0.728	0.740	0.726
75	0.008	0.020	0.122	0.569	0.673	0.672
87.5	0.216	0.590	0.618
100	0.005	0.020	0.076	0.478	0.561
112.5	0.036	0.319	0.501
125	0.007	0.020	0.164	0.436
137.5	0.085	0.367
150	0.295
162.5	0.222
175	0.158
200	0.077

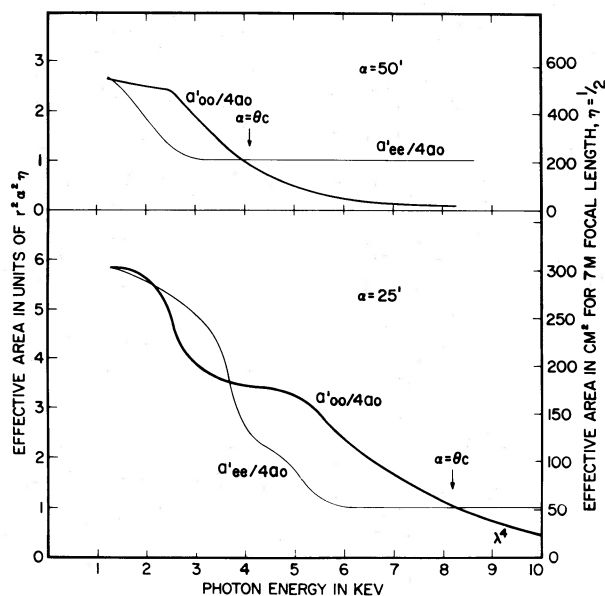


FIG. 4.—Theoretical effective area of nickel reflectors with w/l equal to $25'$ and $50'$. The area for the true focus is given by the thicker line, for the diffuse component by the thinner. Each arm of the cross focus has an effective area equal to the geometric mean of the plotted values. Areas for a 7 m focal length telescope are given by the right-hand scale.

for $\alpha = 50'$, the effective area for each component is equal to $r^2\alpha^2\eta$. This does not fall far short of the maximum possible area of $\pi r^2\alpha^2$ for an ideal grazing-incidence telescope of nested parabolas, with all frontal area focusing parallel light to a single image. For energies in the range from E_c down to $\frac{1}{2}E_c$ the effective area for the true image rises to about 3 times the critical value, and amounts to between one-fourth and one-third of all the energy received by the detector. The effective area for $\alpha = 25'$ is relatively constant from 1 to 5 keV, and still as much as 20% of its peak value at 8 keV. The 50' mirror has less area above 4 keV, but is about twice as efficient at low energies (remembering α^2 is 4 times larger). We have estimated the effective area in the band 44–60 Å using the low-energy reflectivities given by Giacconi *et al.* (1969) and find values for each of the four image components of $7r^2\alpha^2\eta$ for $\alpha = 50'$ and $14r^2\alpha^2\eta$ for $\alpha = 25'$.

b) Angular Resolution

The resolution of the telescope is set by three factors: spherical aberration, diffraction at the cells, and the projected size of the cell. Spherical aberration limits the angular resolution to an angle $\Delta\theta_s = 3200 F^{-3}$ seconds of arc, where F is the effective focal ratio of the focal length to the working aperture, which depends on wavelength. The smallest focal ratio at a given wavelength is $\sim 2^{-1/2}\theta_c$, corresponding to edge rays that are incident at θ_c on both cell walls. Adopting the value of θ_c given above for nickel, we obtain

$$\Delta\theta_s \text{ (seconds of arc)} = 8 \times 10^{-3} \lambda^3 \text{ (Å)}. \quad (7)$$

The spherical aberration is thus a maximum of $1''$ at 5 Å while at 20 Å , where the critical angle is $5^\circ 5'$, and a focal ratio $f/3.7$, the aberration is $1'$. We note that if the cells have $\alpha \ll \theta_c$, then in fact the focal ratio will not be as fast as indicated above, because multiple reflections will result in low reflectivity near the grazing angle.

The limits to angular resolution of the telescope set by cell size are the geometric limit, equal to the ratio of cell size w to the focal length f , and the diffraction limit, equal to λ/w . For a given focal length and wavelength, the highest resolution is achieved by choosing the cell size to equalize the geometric and diffraction limits, i.e.,

$$w = (\lambda f)^{1/2}, \quad (8)$$

when the angular resolution $\Delta\theta_d$ is given by

$$\Delta\theta_d \approx (2\lambda/f)^{1/2}. \quad (9)$$

Given the extraordinary efficiency of evolutionary development, it is no surprise that cell size in the lobster eye is close to satisfying this criterion. The measured cell width is $\sim 67 \mu\text{m}$, while for the focal length of $\sim 1500 \mu\text{m}$ at a wavelength of $0.55 \mu\text{m}$, equation (8) yields $w = 29 \mu\text{m}$. The resolution of $2:5$ set by the cell size is equal to the spherical aberration for a focal ratio $f/0.7$. Again from the relations above, this corresponds to a critical angle of 0.5 rad, close to the value of $\alpha = 0.5$ for a macruran eye (Land 1978).

The limits to resolution set by cell size in X-ray telescopes can in principle also closely match those set by spherical aberration. At 5 Å , for example, a telescope of focal length 10 m has a maximum resolution set by equation (9) of $2'0$ for a cell width of $70 \mu\text{m}$. If arrays of cells of this width could be built, they would allow the construction of a telescope with field and spatial resolution similar to that recorded on Palomar sky survey plates. The manufacture of arrays of cells of such width, and length of $\sim 1 \text{ cm}$, constitutes a major technological challenge. Not only is the scale small, but very exacting tolerances in surface smoothness, flatness, and accuracy of the square geometry must be met.

c) Fabrication

We have given some thought to the possible methods of fabrication. Because the same optical element is repeated many times, it would obviously be desirable to use some sort of replication technique. However, in order to achieve reflectivities as close as possible to the theoretical values of Table 1, it may be necessary to use fused silica or glass surfaces with very high quality finish. A brute-force approach to the construction of a telescope with cells of 1 mm width would make use of thin plates (0.2 mm), polished with a slight wedge angle. For $r = 10 \text{ m}$ and $w = 1 \text{ mm}$ the wedge should be 4 fringes per cm at 5461 Å . Some of these plates would be made into parallel strips of width equal to the cell width, and then glued in a fan pattern to a plate with a precision jig and very little

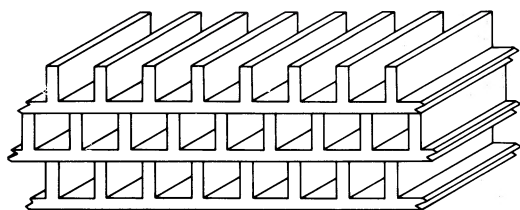


FIG. 5a

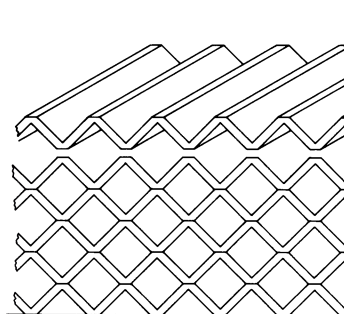


FIG. 5b

FIG. 5.—Two possible arrangements of square cells in a subarray.

glue. Fans prepared in this way would be nickel-coated on both sides, and then stacked together as shown in Figure 5a to make subarrays of a few inches square. Subarrays would then be attached to a honeycombed spherical support surface. If cells on a 1 mm grid are used, then each square meter of aperture requires several hundred square meters to be polished and a million strips to be fabricated and glued. Automated production with machine-operated assembly would be essential. A more attractive approach to construction would be to electroform or mould the subassemblies from rigid plastic. Recent research indicates that good X-ray reflectivity can be achieved in electroformed surfaces. It is not clear how small a cross section for the cells could be achieved. One millimeter would seem to be not unreasonable, but perhaps substantially smaller sizes, approaching the ideal sizes of $100 \mu\text{m}$ set by diffraction, would be possible, depending on the replication method. Figure 5b shows how small square cell arrays might be assembled from electroformed corrugated sections.

A general property of the mirror is that once a practical construction method is developed, there is no reason why a rather large mirror of 2–3 m in diameter should not be made. It need not be any heavier than a large normal-incidence mirror of similar aperture and requires only a large honeycomb support, and much replication.

III. A LABORATORY MODEL

As a demonstration of the imaging properties described above we have constructed a simple model and made photographs in visible light at the image plane. The model incorporated a single square cell 4.5 mm on a side, made from uncoated microscope

slides 76 mm long. The value of w/l of 0.059 for this box was chosen so that the falloff of reflectivity at the glass/air interface with increasing grazing angle would to some degree simulate the behavior of X-ray reflection at a metallic surface. For equations (1) given above, $\alpha = w/l = 3^\circ 40'$, and the appropriate reflectivities given by the Fresnel relations, with $n = 1.5$ and for unpolarized light, are $R(\alpha) = 0.092$, $R(2\alpha) = 0.84$, $R(3\alpha) = 0.78$, $R(4\alpha) = 0.71$, $R(5\alpha) = 0.44$, $R(6\alpha) = 0.37$. The effective areas in the different modes from equations (1) are all given by the same value of A , equal to 4.67.

The single cell was supported by a rectangular frame at a distance of 1.14 m from a spherical bearing, with the cell axis along a line to the bearing center. A full lens was simulated by moving the axis in a raster while making a time exposure at the focal plane. Photographs were obtained of two distant slide projectors of different intensity at an angular separation of $4^\circ 1'$. Photographic enlargement paper was exposed at the focus for 1 minute while the cell was rastered over a ~ 25 cm aperture to obtain the image given in Figure 6. The central images were overexposed to bring up the diffraction-like linear images, forming a cross through the central image. The difference in character between the horizontal and vertical images is due in part to the poor geometry of the cell, and in part to the hand-generated raster scan, which was not very smooth in the horizontal direction. If the cell had been more accurately constructed, the central spot diameter would have been smaller, equal to the cell diagonal of 6.4 mm. Despite these imperfections, however, the laboratory model does serve to illustrate the character of the images that are obtained with this type of optics.

IV. APPLICATION TO ASTRONOMY

Several unique properties make the square-cell telescope well suited for X-ray astronomy from satellites. Perhaps the most interesting is its potentially unlimited field of view, since X-ray telescopes currently used and proposed have fields limited to about 1° , the angle of grazing incidence. To realize in practice a very wide field would require a spherically curved imaging detector as in wide-field Schmidt telescopes. However, because of the rather slow focal ratio at the X-ray focus, a flat detector can accommodate a substantial field of view before the blur from field curvature becomes severe. One can show that for an optimally located focal plane, the maximum blur diameter is given in angle by $\theta^2/16f$, where θ is the full angular field in radians and f the focal ratio. For a 10° field and a focal ratio $f/8$ set by the reflectivity cutoff, the maximum blur is $50''$, occurring at the center and edges of the field. When higher resolution or larger field is required, the detector could be segmented into smaller flat regions approximating the curved focal plane. An imaging proportional counter detector of four square components might be made with very little loss at the joints, since electrical connections can be made at the outside edges to both horizontal and vertical wires in each quadrant.

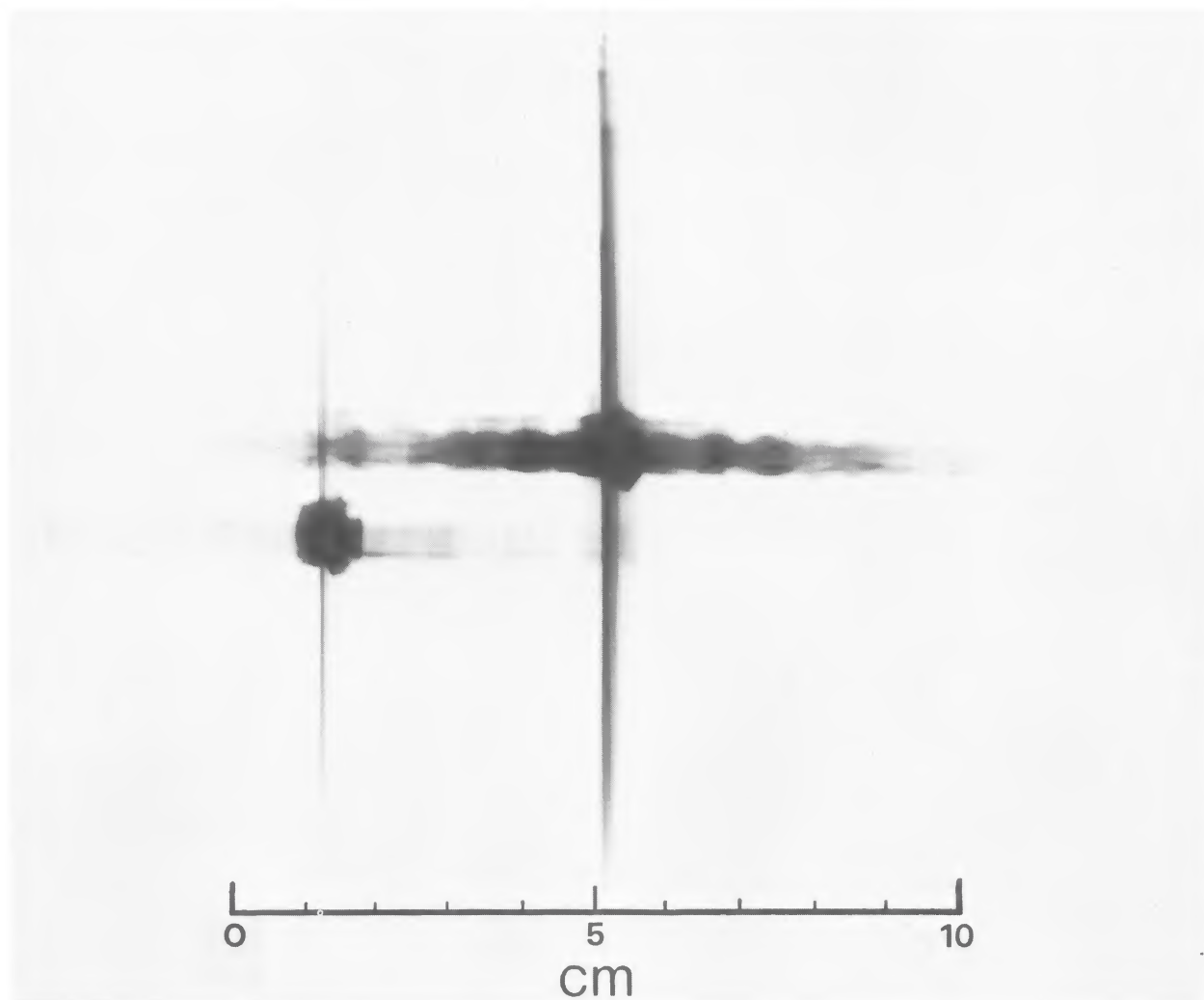


FIG. 6.—Image of two distant point sources obtained with a model telescope of 57 cm focal length described in the text. The diffraction-like lines passing through the point focus are characteristic of the optics. While macruran crustaceans have been seen by such images for millions of years, this is to our knowledge the first photographic record made with square cell optics.

A second and important characteristic of these optics is the wide energy or wavelength response. There are two ways in which the high-energy response is improved over conventional X-ray optics. First, it is quite practical to use small grazing angles, since these only involve making the cells longer. The structural problems and difficulty of fabrication are not substantially increased. Second, the reflection geometry is such that, while the effective area of the true focus drops as λ^4 below the critical wavelength, there is present a high energy flux in the cross image which falls off only as λ^2 (eq. [6]). For many sources the cross image will be detectable above background, and can be used to determine the spectrum in the wavelength range $\frac{1}{2}\lambda_c - \lambda_c$. In this way the useful focused response can be extended well past the important iron line emission region at ~ 7 keV. At still higher energies the directly transmitted radiation gives a low-resolution image of angular resolution 2α . The effective area of $r^2\alpha^2\eta$ is independent of wavelengths up to energies where the cells become transparent, $E \lesssim 50$ keV. This image could be recorded by a sealed low-resolution detector, with a relatively thick beryllium window, underlying the primary high-resolution detector.

At low energies, multiple reflections in the cells serve to increase the effective area of the telescope, each pixel collecting radiation from a much larger fraction of the mirror than at high energy. This is illustrated by path A in Figure 2. Very efficient use is thus made of the frontal area, the same cell surfaces working at a wide range of grazing angles. In currently used optics, a large collection area at low energy requires surfaces with large grazing angles, and this requirement limits the effectiveness in collecting high-energy radiation.

The possibility of obtaining with one exposure spectra from 0.1–50 keV of all brighter objects in a large field of view is valuable, since the X-ray sky is so variable. High-energy and low-energy observations a year or even a day apart cannot be combined to give reliable spectra of many sources.

Against these advantages we must weigh the problem of reduced contrast of high-resolution images caused by the extra radiation transmitted by the mirror. How do the linear and diffuse image components degrade the performance, compared to that of a pure imaging telescope? Consider the effect of the diffuse X-ray background. An unresolved stellar object will have to be detected against this background, which relative to star is about 4 times brighter than for a perfect telescope, because all the image components contribute. At first sight this would appear to be a substantial drawback; however, we can show that even when so intensified the background still gives a very low counting rate, comparable to the non-X-ray counting background induced in the detector by cosmic rays.

The effective area for the diffuse background is equal to $(a_{ee}' + a_{eo}' + a_{oe}' + a_{oo}')r^2\alpha^2\eta/4a_o$. For an optimally matched detector, in which the pixel size is set equal to the cell width w , each pixel subtends on the sky a solid angle $(w/f)^2$. Let the flux of the diffuse

background be B photons $\text{cm}^{-2} \text{s}^{-1} \text{sr}^{-1} \text{keV}^{-1}$. The rate R of photons incident per pixel will then be equal to $Bw^2\alpha^2\eta(a_{ee}' + a_{eo}' + a_{oe}' + a_{oo}')/a_o$ photons $\text{s}^{-1} \text{keV}^{-1}$. Note that this expression depends only on the cell dimensions and coating, and is independent of both telescope aperture and focal length. As an example, we calculate R for $\alpha = 50'$ and the values for a' appropriate for a nickel-coated mirror given in Figure 4. We choose $w = 1$ mm, $\eta = 1/2$, and B equal to $8.5E^{-1.4}$ above 1 keV, 100 at 0.25 keV. These values yield $R(3 \text{ keV}) = 5 \times 10^{-5} \text{ keV}^{-1}$, $R(1 \text{ keV}) = 4 \times 10^{-4} \text{ keV}^{-1}$ and $R(0.25 \text{ keV}) = 3 \times 10^{-3} \text{ keV}^{-1}$. These rates should be compared with the cosmic-ray background rates estimated for the *HEAO 2* imaging proportional counter by Giacconi, Schreier, and Seward (1978). Again for 1 mm pixels these are 1.5×10^{-3} counts per second for each of the bands 0.1–1.5 keV and 1.5–4 keV. In the same bands the diffuse background contribution calculated above would be about 1.5×10^{-3} and 0.5×10^{-3} counts per second, respectively. Thus we find for this detector that the limiting magnitude for very long exposures is set primarily by detector noise, and the intensified diffuse background is of little consequence, at least above 1 keV. For moderate exposures of around 1 hr the noise from all sources amounts to only a few counts, and will be insignificant for any source giving a few tens of photons, the minimum for crude photometry and colors. The fact that the background rates are so low means that the limiting sensitivity to isolated faint sources cannot be markedly improved by reducing the pixel size. Cell sizes of a millimeter or somewhat less are adequately small for finding and measuring faint objects.

We have not considered in any detail how images could be processed to reconstruct true X-ray maps of large, complex, extended emission regions. While such processing will inevitably increase graininess and noise in an image, it would seem to be fairly straightforward, compared, say, to the image synthesis from one-dimensional scans that has been done for the Cygnus Loop (Stevens and Garmire 1973; Rappaport *et al.* 1974). As we have seen, the linear and diffuse components do not extend over the whole telescope field, which might be 8° – 10° , but have a width equal to twice the grazing angle (except at low energy). The raw image will show a high-resolution (cell-limited) image superposed on a blurred background image. Very faint sources near the galactic plane could fall under the cross component of the image of a bright galactic source, but, as in the problem of seeing Sirius's white dwarf companion, the linear diffraction-like image can be shifted by rotating the telescope.

To illustrate the potential for X-ray astronomy, we consider first the performance of a square-cell telescope that could be launched by the shuttle to make a deep survey of the entire sky, analogous to the Palomar sky survey in the optical. Such a telescope would be complementary to the planned 1.2 m high-resolution Wolter telescope, which would have a small field with very high spatial resolution. We choose an aperture of 2.5 m square and a focal length

of 7 m, similar to the dimensions of the space telescope (ST). Vignetting in the field of view of such a telescope results in a 50% loss at the edges of a 10:2 square field. Suppose the detector is 8° square; then the whole field is unvignetted for higher energies, and has about 30% edge droop for long wavelengths. Some 700 exposures will be required to make the complete sky survey. In a two-year mission this would require one per day, and about 5×10^4 s of live time should be possible for each. With a quadrant detector as discussed above, the resolution limit set by field curvature would be about 8". Each detector quadrant, viewing 4°, would need to be 50 cm square.

Imaging proportional counters would be ideal for this telescope. They have quantum efficiency near unity and spectral resolution adequate to resolve iron emission lines, and they have already been built with a resolution of ~ 1 mm and dimensions of ~ 6 cm for the *HEAO* telescope. Recently Gorenstein *et al.* (1979) has demonstrated a 10 cm² sealed detector with spatial resolution better than 1 mm and good spectral resolution. Imaging detectors of 50 cm would be considerably larger than those that have been and are being used in X-ray astronomy, but high-resolution proportional chambers of comparable complexity and size are built and used in particle physics. A proportional counter with a spatial resolution of 1 mm would yield an angular resolution of 29" on the sky. The mirror elements should then be somewhat less than 1 mm² to avoid further degradation of resolution.

The choice of cell aspect ratio depends on the importance we attach to high-energy response. We choose $\alpha = 25'$ to illustrate the good response that can be achieved at the iron lines. The effective collecting area for the point, cross, and diffuse images can then be derived from § II, and are given by the right-hand vertical scale in Figure 3. For the point image, the effective area is 1450 cm² at 50 Å and holds up well out to 6 keV, dropping from 320 to 120 cm² over the range 1–6 keV. Above 6 keV it drops fairly steeply to 22 cm² at 10 keV. For sources bright enough for the cross image to be detected, the effective area of the cross and point images together is 4000 cm² at 50 Å, 1000 cm² at 1–2 keV, 300 cm² at 6 keV, and still 100 cm² at 10 keV. The directly transmitted diffuse component has a constant effective area of of 50 cm² above 6 keV.

The performance of such a telescope can be compared with that of Kirkpatrick-Baez crossed plate designs. A design for a reflector of this type with comparable total length and resolution has been described in detail by Van Speybroek, Chase, and Zehnpfennig (1971). It has a focal length of 7.9 m and an aperture of 0.96 m diameter, and it was designed to have an on-axis resolution of 30". For an on-axis object it has a similar wavelength response and about 3 times the effective area of the true focus of the 7 m cell telescope with $\alpha = 50'$, given in the upper plot of Figure 4. The total focused energy in the 1–6 keV range (point and cross images together in the cell telescope) is about the same for both types, as one would expect for telescopes of the same total length.

The principle difference is that in the cross-plate design the performance deteriorates rapidly for objects off axis. At 15' off axis the effective area is halved, and the theoretical resolution is degraded to 1:3.

The crossed-plate design is thus best suited to the construction of telescopes required to have very large collecting area if a large field of view is not important. Many such reflectors, each with its own detector, are used in the large-area modular array reflector (LAMAR) proposed by Gorenstein (1978). The effective area of the array is 1 m² at 1–2 keV, an order of magnitude larger than that for the total image flux of the square-cell telescope of the same frontal area (6 m²) considered above. The square-cell telescope, with a well-focused field 100 times larger, is better suited for survey work, and for discovering burst activity. In the suggested 2 year survey mission, it could survey the whole sky to the limiting sensitivity of the deepest maps from the *Einstein* (*HEAO 2*) telescope.

As another example of a square-cell telescope for shuttle launch, we consider an all-sky monitor very similar in geometry to a real lobster eye, a hemisphere of diameter 3 m covered with cells of width $\lesssim 1$ mm. The image scale at the focal hemisphere of 75 cm radius is 4.6 mm⁻¹. Each star would give a 1 mm point image centered in a cross of 2 cm diameter. A detector with 1 mm resolution could thus resolve sources 5' apart, and give positions of isolated sources to $\sim 1'$ precision. With a cell aspect ratio α of 50', the effective area at 1–3 keV would be 1.5 cm² for the 5' image and 2 cm² for the cross, assuming a frontal efficiency of 0.5. This telescope could survey the sky to the limiting sensitivity of *Uhuru* in an hour, and would be able to locate even quite faint (3×10^{-8} ergs cm⁻²) burst sources to a precision of 2'–3'.

V. CONCLUSION

In conclusion, we recognize that further study is needed in several areas before telescopes of the type described could be considered for satellite astronomy missions. Most important, practical techniques must be developed for fabricating square-cell arrays, and achieving in them X-ray reflectivities close to those predicted by theory. Another substantial laboratory effort is required to make large proportional counter detectors which combine both good spatial and good spectral resolution. Finally, it would be very desirable to model by computer the results that could be achieved in mapping diffuse emission by deconvolving the cross response, taking account of the limitations of event statistics.

I am grateful to Drs. Richard Allen and Peter Martin for assistance in obtaining the photograph in § III, to Drs. Paul Gorenstein, Herb Gursky, Bruce Margon, and Peter Stockman for valuable discussions of this concept, and to the NSF for financial support under grant AST 7822714.

REFERENCES

- Giacconi, R., Reidy, W. P., Vaiana, G. S., Van Speybroek, L. P., and Zehnpfennig, T. F. 1969, *Space Sci. Rev.*, **9**, 3.
- Giacconi, R., and Rossi, B. 1960, *J. Geophys. Res.*, **65**, 773.
- Giacconi, R., Schreier, E. J., and Seward, F. D. 1978, *HEAO B Summary of Instrument Performance (CFA/HEA 78-214)*.
- Gorenstein, P. 1978, in *New Instrumentation for Space Astronomy*, ed. Van der Hucht and Vaiana (London: Pergamon).
- Gorenstein, P., Gursky, H., Harnden, F. R., DeCaprio, A., and Bjorkholm, P. 1975, *IEEE Trans.*, NS-22, p. 616.
- Gorenstein, P., Perlman, D., Parsignault, D., and Burns, R. 1979, *IEEE Trans.*, NS-26, in press.
- Gursky, H., and Schwartz, D. 1974, *X-ray Astronomy*, ed. R. Giacconi and H. Gursky (Dordrecht: Reidel).
- Kirkpatrick, P., and Baez, A. V. 1948, *J. Opt. Soc. Am.*, **38**, 766.
- Land, M. F. 1978, *Scientific American*, **239**, 126.
- Rappaport, S., Doxsey, R., Solinger, A., and Borke, R. 1974, *Ap. J.*, **194**, 329.
- Schmidt, W. K. H. 1975, *Nucl. Inst. Methods*, **127**, 285.
- Stevens, J. C., and Garmire, G. P. 1973, *Ap. J. (Letters)*, **180**, L19.
- Underwood, J. H. 1975, *Space Sci. Instr.*, **1**, 289.
- Vaiana, G. S., Krieger, A. S., Petraso, R., Silk, J. K., and Timothy, A. F. 1974, *Proc. Soc. Photo-Opt. Inst. England*, **44**, 175.
- Van Speybroek, L. P. 1977, *Proc. Soc. Photo-Opt. Inst. England*, **106**, 136.
- Van Speybroek, L. P., Chase, R. C., and Zehnpfennig, T. F. 1971, *Appl. Optics*, **10**, 945.
- Vogt, K. 1975, *Zs. Naturforschung*, **300**, 691.
- Wolter, H. 1952, *Ann. Phys.* **10**, 94.

J. R. P. ANGEL: Steward Observatory, University of Arizona, Tucson, AZ 85721